Nanoscale

PAPER

View Article Online
View Journal | View Issue



Cite this: *Nanoscale*, 2015, **7**, 19557

# A multifunctional role of trialkylbenzenes for the preparation of aqueous colloidal mesostructured/mesoporous silica nanoparticles with controlled pore size, particle diameter, and morphology†

Hironori Yamada,‡[a] Hiroto Ujiie,‡[a] Chihiro Urata,[a] Eisuke Yamamoto,[a] Yusuke Yamauchi[b] and Kazuyuki Kuroda*[a,c]

Received 4th July 2015,
Accepted 26th September 2015

DOI: 10.1039/c5nr04465k

www.rsc.org/nanoscale

Both the pore size and particle diameter of aqueous colloidal mesostructured/mesoporous silica nanoparticles (CMSS/CMPS) derived from tetrapropoxysilane were effectively and easily controlled by the addition of trialkylbenzenes (TAB). Aqueous highly dispersed CMPS with large pores were successfully obtained through removal of surfactants and TAB by a dialysis process. The pore size (from 4 nm to 8 nm) and particle diameter (from 50 nm to 380 nm) were more effectively enlarged by the addition of 1,3,5-triisopropylbenzene (TIPB) than 1,3,5-trimethylbenzene (TMB), and the enlargement did not cause the variation of the mesostructure and particle morphology. The larger molecular size and higher hydrophobicity of TIPB than TMB induce the incorporation of TIPB into micelles without the structural change. When TMB was used as TAB, the pore size of CMSS was also enlarged while the mesostructure and particle morphology were varied. Interestingly, when tetramethoxysilane and TIPB were used, CMSS with a very small particle diameter (20 nm) with concave surfaces and large mesopores were obtained, which may strongly be related to the initial nucleation of CMSS. A judicious choice of TAB and Si sources is quite important to control the mesostructure, size of mesopores, particle diameter, and morphology.

## 1. Introduction

Mesoporous silica nanoparticles (MSN) are promising for various potential applications through effective use of designed mesopores by nanoscale downsizing of mesoporous silica having various characteristics, such as high surface area, high pore volume, tunable mesopores, easiness of surface modification, and mechanical and chemical stabilities.[1–18] MSN are expected to be applied in a wide variety of fields (adsorption, separation, drug delivery, and catalysis) because MSN also have colloidal characteristics, such as dispersity, transparency, and fluidity.[19–37] In addition, their properties and potentialities geared for applications have stimulated the development of the control in the composition, structure, and morphology of MSN.[38–46]

In particular, the control of pore size of MSN is quite important because it affects both the accessibility of in-coming guest molecules and the confinement effect of pores.[47–54] The control of particle diameter of MSN also has a great significance in terms of the uptake, cytotoxicity, and dispersity of MSN.[55–64] Thus, both the control of pore size and particle diameter of MSN is largely meaningful for the precise preparation of different types of MSN appropriate to various applications.

It has already been known that the pore size of mesoporous silica (including MSN) can be enlarged by adding substances, like alkanes, alcohols, and trialkylbenzenes (TAB), into amphiphilic molecules or varying experimental conditions including the concentration of surfactants and the kinds of catalysts.[46–51,63,65–75] One of the most frequently used expanders is TAB such as 1,3,5-triisopropylbenzene (TIPB) or 1,3,5-trimethylbenzene (TMB).[76–78] TAB can enlarge the pore size of MSN easily under basic conditions where it is easy to form MSN.[47,50,75,79] Also, other particulate characteristics such as pore arrangement and particle diameter are varied by using TAB.[47,50,75] In particular, it is quite reasonable to expect that the particle diameter of MSN can be enlarged by using the hydrophobicity of TAB. This is because the appropriate intro-

[a]*Department of Applied Chemistry, Faculty of Science and Engineering, Waseda University, Ohkubo 3-4-1, Shinjuku-ku, Tokyo, 169-8555, Japan. E-mail: kuroda@waseda.jp; Fax: +81-3-5286-3199; Tel: +81-3-5286-3199*
[b]*World Premier International (WPI) Research Center, International Center for Materials Nanoarchitectonics (MANA), National Institute for Materials Science (NIMS), 1-1 Namiki, Tsukuba, 305-0044, Japan*
[c]*Kagami Memorial Research Institute for Material Science and Technology, Waseda University, Nishiwaseda 2-8-26, Shinjuku-ku, Tokyo, 169-0051, Japan*
†Electronic supplementary information (ESI) available. See DOI: 10.1039/c5nr04465k
‡H. Yamada and H. Ujiie contributed equally.

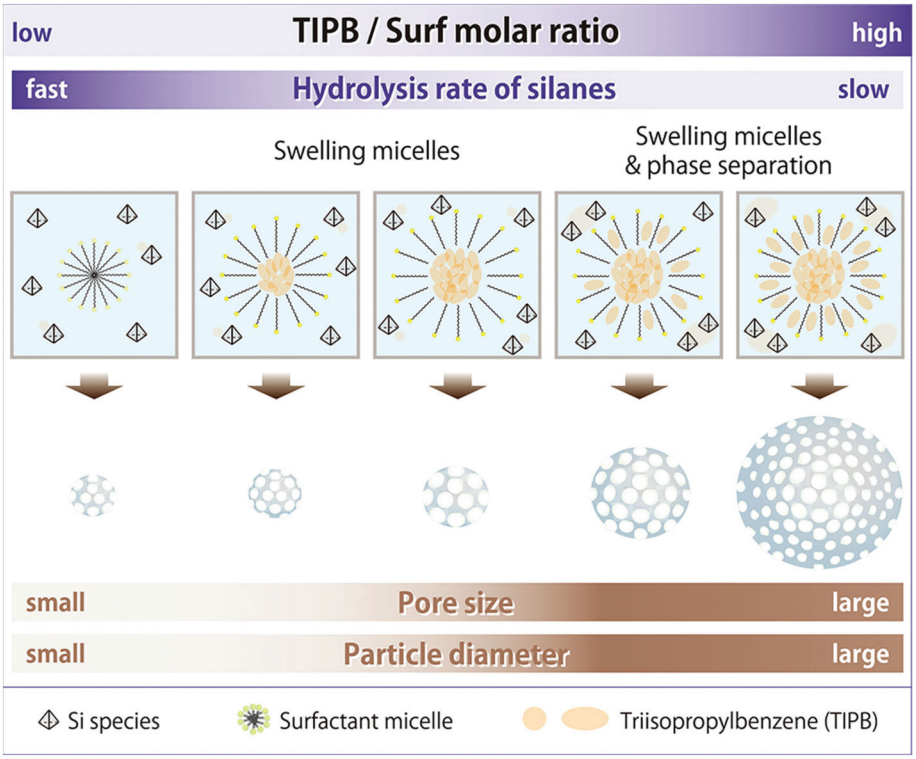


**Scheme 1** Effect of TIPB on the preparation of CMSS.

duction of hydrophobicity into the reaction media can affect the hydrolysis rates of alkoxysilanes, followed by the variation of dominance between nucleation and particle growth.[80] However, how the differences in the amount and kind of TAB affect the pore size, pore arrangement, and particle diameter has not yet been clarified.

In this study, it has been clearly confirmed how trialkylbenzenes play a multifunctional role in the pore size, particle diameter, and morphology of colloidal mesostructured and mesoporous silica nanoparticles (CMSS and CMPS, respectively) under basic conditions (please see Scheme 1). As TAB, 1,3,5-triisopropylbenzene and 1,3,5-trimethylbenzene were used, and as Si sources, tetrapropoxysilane (TPOS) and tetramethoxysilane (TMOS) were used. When TIPB was used as TAB and TPOS as a Si source, both the pore size (from 4 nm to 8 nm) and particle diameter (from 50 nm to 380 nm) were enlarged, depending on the amount of TIPB. When an excess amount of TMB was used as TAB, the pore size of CMPS was enlarged above 10 nm, but the mesostructure and particle morphology were varied. When TMOS and TIPB were used, CMPS with a small particle diameter (20 nm), concave surfaces, and a large pore size (5–8 nm) were obtained, and they should be equivalent to particles at the initial nucleation. Thus, TAB played an important role in the enlargement of the pore size and diameter of particles as well as in the variation of the morphology. The differences in the mesostructure and particle diameter of CMSS by TAB should be ascribed to the larger molecular size and higher hydrophobicity of TIPB than those of TMB, which indicates the different interactions between surfactant micelles and TAB. Moreover, removal of surfactants and TAB by a dialysis process was successfully achieved by modifying the dialysis process reported previously by us. These findings can provide a method to control both the pore size and particle diameter of aqueous porous particles. This leads to the development of siliceous materials which can contain more and larger guest molecules and can reduce the nanorisks of toxicity toward applications for drug delivery, bioimaging, and catalysis.

## 2. Experimental section

### 2.1 Materials

Cetyltrimethylammonium bromide (CTAB) and triethanolamine (TEA) were purchased from Wako Pure Chem. Ind., Ltd. Tetramethoxysilane (TMOS: $Si(OCH_3)_4$), tetrapropoxysilane (TPOS: $Si(OC_3H_7)_4$), 1,3,5-trimethylbenzene (TMB) and 1,3,5-triisopropylbenzene (TIPB) were purchased from Tokyo Kasei Co., Ltd. Acetic acid (AcOH), ethanol (EtOH), and 2-propanol (2-PrOH) were purchased from Kanto Chem. Co., Inc. A sheet of high density polyethylene (HDPE) was purchased from PlaPort Co. Ltd. All substances were used without any further purification.

### 2.2 Characterization

TEM images were recorded on a Jeol JEM-2010 microscope operating at 200 kV. SEM images were obtained on a Hitachi

 

S-5500 electron microscope operated at an acceleration voltage of 5–30 kV. Samples for TEM and SEM measurements were dropped and dried on a carbon-coated micro-grid (Okenshoji Co.). X-ray diffraction (XRD) patterns of dried powder samples were obtained on a Rigaku Ultima IV with Fe Kα radiation (40 kV, 30 mA). Nitrogen gas adsorption–desorption measurements were performed with an Autosorb-2 instrument (Quantachrome Instruments) at −196 °C. Samples were pre-heated at 120 °C for 24 h under $1 \times 10^{-2}$ Torr. Brunauer–Emmett–Teller (BET) surface areas were calculated from adsorption data in the relative pressure range from 0.05 to 0.20. Pore volumes were calculated at $P/P_0 = 0.95$. Pore size distributions were evaluated using the adsorption branch with non-local density functional theory (NLDFT). Thermogravimetry-differential thermal analysis (TG-DTA) was carried out with a Rigaku Thermo Plus 2 instrument under a dry air flow at a heating rate of 10 °C $min^{-1}$ up to 900 °C. IR spectra were obtained by using a Jasco FT/IR 6100 spectrometer by a KBr disk method. Dynamic light scattering (DLS) measurements were conducted with a Horiba Nano Partica SZ-100-S at room temperature. The $\zeta$-potential measurements were conducted with an Otsuka Electronics ELSZ-1 at 20 °C.

### 2.3 Preparation of colloidal mesostructured silica nanoparticles (CMSS) by adding trialkylbenzenes

**2.3.1 Preparation of CMSS without the addition of TAB.** According to previous reports,[80–86] CMSS were prepared by tetraalkoxysilanes (TPOS or TMOS). First, TEA (0.420 g), and CTAB (2.00 g) were added to 240 ml of water (solution 1). Next, solution 1 (pH 9.5) was stirred at 80 °C for 2 h. Then 11 mmol of tetraalkoxysilanes (TPOS or TMOS) was added to solution 1 and the mixture was stirred vigorously at 80 °C for 12 h to become a colloidal state. Finally, the colloidal suspension (pH 8.2) was filtered with filter paper (No. 5). The molar ratio of the precursor solution was 1 tetraalkoxysilane : 0.50CTAB : 0.25TEA : 1200$H_2O$. The samples are denoted as P-as and M-as, corresponding to TPOS and TMOS, respectively. The phrase "as" means "as-synthesized" or "before removal of surfactants".

**2.3.2 Preparation of CMSS by using TIPB and TPOS.** By varying the value of $x$ which stands for the molar ratio of TIPB to CTAB, CMSS were similarly prepared, as shown above (1). A certain amount of TIPB (5.5$x$ mmol: $x$ = 0.2, 0.4, 0.8, 2, 4, 8, and 20) was added to a precursor solution 1 (that is, solution 2), and solution 2 was stirred for 30 min. Then, 11 mmol of TPOS was added to solution 2 and the mixture was stirred at 80 °C for 12 h to become a colloidal state. Finally, the colloidal suspension was filtered with filter paper (No. 5). When the value of $x$ was 0.8, an oil phase derived from TIPB was observed on the surface of the colloidal solution. With further increase in the value of $x$, an oil phase was observed on the surface of the main aqueous phase. A portion of the oil phase was found on the filter paper on filtration for those cases. This means that the amount of TIPB in the filtrates was not always the same as the initial amount. The samples are denoted as P_TIPB$x$-as.

**2.3.3 Preparation of CMSS by using TMB and TPOS.** Another type of CMSS was also prepared by using TMB as TAB, instead of TIPB. The amount of TMB was 5.5$x$ mmol ($x$ = 0.8 and 20). The samples are denoted as P_TMB$x$-as.

**2.3.4 Preparation of CMSS by using TIPB and TMOS.** The other type of CMSS was similarly prepared by using TIPB as TAB and TMOS as a Si source. The amount of TIPB was 4.4 mmol (5.5$x$ mmol ($x$ = 0.8)) and that of TMOS was 11 mmol. The sample is denoted as M_TIPB-as.

### 2.4 Removal of surfactants and TAB by a dialysis process

In order to remove surfactants and TAB, a dialysis process was conducted in the same way as shown in our previous papers.[80–82,84–87] A colloidal suspension (50 mL) of one of the following ones (P-as, M-as, P_TIPB$x$-as, P_TMB$x$-as, or M_TIPB-as) was transferred into a dialysis membrane tube composed of cellulose (molecular weight cut off = 12 000–14 000) and dialyzed for 12 h against 250 mL of a mixture containing 2 M acetic acid and 2-propanol (1 : 1, v/v) and this process was repeated five times. Then the tube, which contained CMPS, was immersed in water to remove AcOH/2-PrOH from the tube, and the process was repeated twice. Finally the pH value of the resulting solution was 3.4. The samples are denoted as P-dia, M-dia, P_TIPB$x$-dia, P_TMB$x$-dia, or M_TIPB-dia, respectively, where "dia" means "after dialysis" or "after removal of surfactants". The removal of both organics has been proved by the absence of IR peaks due to those organic compounds and by no weight losses due to them, as shown in the TG curves (ESI, Fig. S1 and S2†). In addition, dried samples were obtained by heating a portion of CMPS at 120 °C for 12 h.

### 2.5 Measurement of swelling ratios of HDPE for TMB and TIPB

In order to estimate the extent of affinity of TAB to alkyl chains of surfactants, the swelling ratios of some fragments of HDPE sheets for TMB and TIPB were measured. These ratios were obtained by comparing the initial volume with the swollen volume after an immersion of HDPE fragments in TAB. Each piece was immersed in 1 mL of TAB and shaken at 100 rpm for one week. After the procedure, the pieces were dry-wiped to remove any residual liquid and weighed. Measurements were performed at least 3 times for each sample. The details on the calculation of the swelling ratios are shown in the ESI.†

## 3. Results and discussion

### 3.1 Preparation of CMSS and CMPS with enlarged pore size and particle diameter by adding TIPB

**3.1.1 Characterization of P_TIPB$x$-as.** All types of P_TIPB$x$-as were somewhat transparent with clear Rayleigh and Mie scattering of the colloidal solutions without any aggregation, indicating their high dispersity (Fig. S3†). As the amount of TIPB increased (*i.e.* the increase in $x$), the appearances of P_TIPB$x$-as were more cloudy, suggesting that the

particle diameter became larger. As shown in the distributions of hydrodynamic diameters measured by DLS (Fig. S4†), all types of P_TIPB*x*-as show a single peak and no peaks above 1000 nm are observed. On the basis of these data on the appearances and particle size distributions, it was confirmed that the particle diameter of P_TIPB*x*-as increased with the amount of TIPB and that these CMSS were highly dispersed. Also, the enlargement of the particle diameter (from *ca.* 50 nm for P-as to *ca.* 380 nm for P_TIPB20-as) is shown in the TEM images (Fig. S5†). In terms of mesostructure, the TEM images (Fig. S5†) show that the shape of mesostructure is varied from worm-hole to radially-arranged, as the amount of TIPB increases. These variations of the particle diameter, pore size, and the shape of mesostructure (or pore) will be discussed in section 3.1.3.

**3.1.2 Characterization of P_TIPB*x*-dia.** Removal of surfactants and TIPB by a dialysis process for P-as and P_TIPB*x*-as was well accomplished with the retention of the dispersity of particles (the details are shown in the ESI†). Like the cases of P_TIPB*x*-as, all types of P_TIPB*x*-dia were almost transparent with clear Rayleigh and Mie scattering of the colloidal solution (Fig. S6†). Fig. S7† shows that the particle diameter of P_TIPB*x*-dia increased with the amount of TIPB and that these CMPS were highly dispersed like the cases of the corresponding CMSS. As shown in Fig. 1 and 2, the enlarged particle diameter was retained.

On the basis of the TEM images (Fig. 1), it was also confirmed that the mesostructure was not varied after dialysis. The mean pore size in each particle, roughly estimated by using the SEM images (Fig. 2), varied from *ca.* 4 nm to *ca.* 10 nm with the amount of TIPB, in the range of $x \leq 0.8$. The $N_2$ adsorption–desorption isotherms (Fig. S8†) show type IV isotherms for all types of dried samples of CMPS, meaning that they have mesopores. The relative pressure of capillary condensation for P-dia is $P/P_0 = 0.4$, while in the cases of $x$ = 0.2, 0.4, 0.8, and 2, the values are $P/P_0$ = 0.45, 0.5, 0.6, and 0.65, respectively. The mean pore size of P-dia is 4.3 nm, while in the cases of $x$ = 0.2, 0.4, 0.8, and 2, the pore sizes are enlarged to 4.9 nm, 6.6 nm, 7.0 nm, and 8.1 nm, respectively (Fig. S8†). In this range ($x \leq 2$), TIPB should be incorporated into micelles of surfactants and the micelles are sufficiently swollen. On the other hand, in the range of $2 \leq x < 8$, the relative pressure is $P/P_0 = 0.65$ and the mean pore size is 8.1 nm regardless of the amount of TIPB. This means that the extent of swelling of micelles is limited. Moreover, in the case of $x$ = 20, the mean pore size is 6.8 nm, smaller than those in the cases of $2 \leq x < 8$. The isotherm in this case ($x = 20$) shows that the adsorbed amount of nitrogen is less than those of the cases of other $x$ values and that the shape of isotherm is different from others. An excessive amount of TIPB should lead to the variation of the curvature and the shape of micelles,[88] resulting in the transformation of the structure.

The XRD patterns (Fig. S9†) show that the mesostructure is enlarged to some extent with the amount of TIPB. In the region of $x \leq 2$, the periodicity of structure is varied ($d$ = from 5.6 nm to 9.0 nm). In the region of $2 \leq x < 8$, the variation of the periodicity of structure was not observed. However, in the case of $x = 20$, the periodicity slightly decreased to 7.9 nm. The tendency will be discussed in the next section.

**3.1.3 Enlargement of both the pore size and particle diameter of CMPS by adding TIPB.** The variations of the pore size and particle diameter of CMPS with the amount of TIPB are shown in Fig. 3. The values of particle diameters were obtained from the data in Fig. S4 and S7,† and the values of pore sizes were obtained from the data in Fig. S8.† The overall tendency is divided into two parts. (i) In the range of $0 \leq x \leq 8$, both the pore size and particle diameter are enlarged. While the pore size is enlarged in the range of $0 \leq x \leq 2$ and becomes

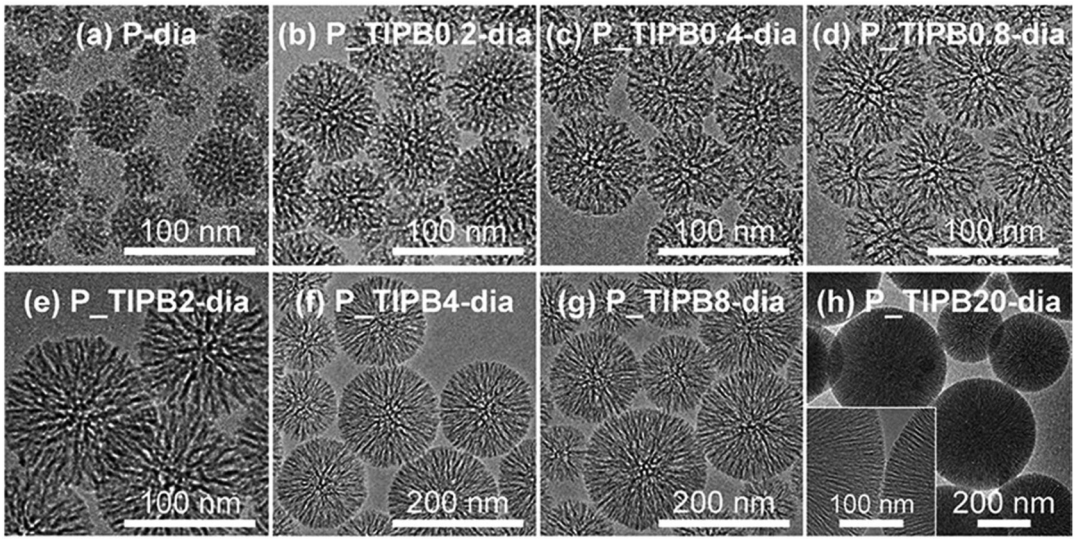


**Fig. 1** TEM images of P_TIPB*x*-dia: $x$ = (a) 0, (b) 0.2, (c) 0.4, (d) 0.8, (e) 2, (f) 4, (g) 8, and (h) 20.

 

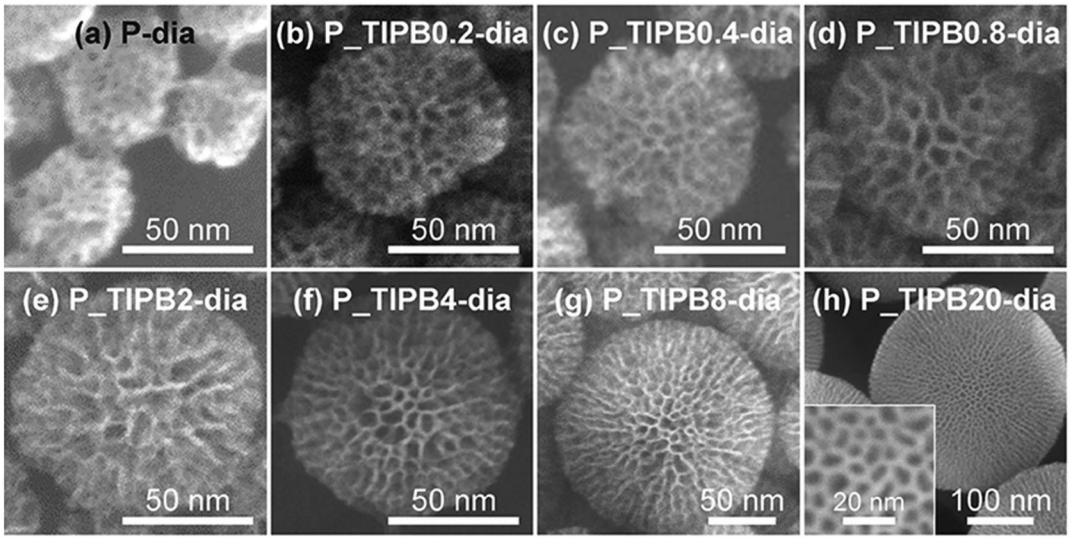


**Fig. 2** SEM images of P_TIPB*x*-dia: *x* = (a) 0, (b) 0.2, (c) 0.4, (d) 0.8, (e) 2, (f) 4, (g) 8, and (h) 20.

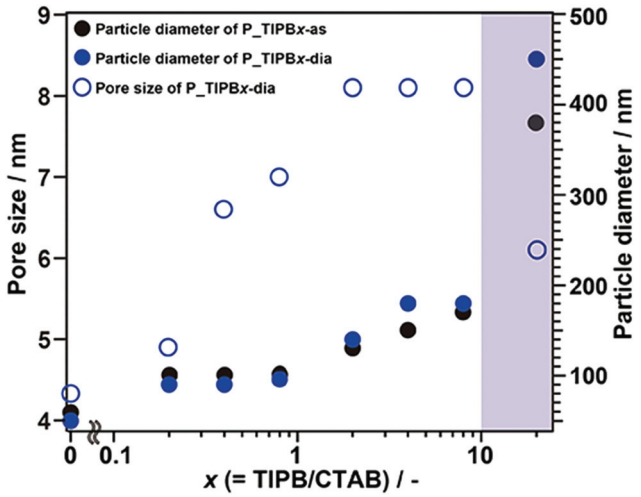


**Fig. 3** Variation of particle diameter and pore size of P_TIPB*x*-dia (*x* = 0, 0.2, 0.4, 0.8, 2, 4, 8, and 20); the particle diameter was obtained from Fig. S4 and S7,† and the pore size was obtained from Fig. S8.

constant over $x = 2$, the particle diameter is gradually and constantly enlarged in this range ($0 \leq x \leq 8$). (ii) In the range of $8 < x \leq 20$, the pore size decreases and the particle diameter is obviously enlarged. In this section, at first, the enlargement of the particle diameter and pore size by adding TIPB in the whole range is explained. Then, the roles of TIPB in the two ranges described above are separately mentioned.

The general view about the enlargement of both the pore size and particle diameter is explained as follows. In terms of pore size, TIPB is incorporated into micelles of surfactants, as reported previously.[76–78,89–91] In terms of particle diameter, the decrease in the hydrolysis rate of alkoxysilanes leads to particle growth more dominant than nucleation.[80,82] In the present case, the interaction of TPOS with TIPB due to hydrophobic interactions should inhibit the contact of TPOS with water. It results in the decrease in the hydrolysis rate of TPOS and then particle growth. After separate descriptions on the following two ranges (sections (3.1.3.i) and (3.1.3.ii)), the present case is compared with the previously reported particle growth by the addition of alcohols (section (3.1.3.iii)).[80]

*3.1.3.i* $0 \leq x \leq 8$. Firstly, the enlargement of the pore size with the increase in the molar ratio of TIPB to CTAB (that is, the value '*x*') is explained. As shown in Scheme 1, when *x* is low ($x \leq 2$), TIPB molecules are probably located at the center of micelles of surfactants. This means that the swelling of micelles is due to the incorporation of TIPB. On the other hand, when *x* is larger ($2 < x \leq 8$), the pore size is not enlarged. In this region, the oil phase of TIPB in the resulting solution was obviously separated from water. This means that, in the case of an excess amount of TIPB, TIPB should be more stable as a separated phase due to the aggregation of TIPB itself than as a solubilized phase in micelles.

Next, the gradual enlargement of the particle diameter is described as follows. In particular, when *x* is low ($x \leq 2$), the enlargement was not clear, but when *x* is larger ($2 < x \leq 8$), the enlargement is clearly shown. In the case of low *x* ($x \leq 2$), the additional TIPB was mainly absorbed into micelles and it was unlikely for TIPB to be separated from water and to come into contact with TPOS. In the case of higher *x* ($2 < x \leq 8$), the phase separation of TIPB as an oil leads to the interaction with TPOS and the lack of contact of TPOS with water. It causes the decrease in the hydrolysis rate of TPOS as shown in Scheme 1, followed by particle growth more dominant than nucleation. This phenomenon is similar to the previous study[80] in which the addition of alcohols (typically butanol) leads to the decrease in the hydrolysis rates of alkoxysilanes and the

increase in the particle growth. Moreover, the enlargement of the particle diameter ($0 < x \leq 2$) compared to the particle diameter at $x = 0$ is due to a slight interaction of TIPB with TPOS, although most of TIPB is absorbed into micelles. This enlargement is also explained by the decrease in the hydrolysis rate of TPOS.

Consequently, when $x$ is low ($x \leq 2$), the pore size is evidently enlarged due to the incorporation of TIPB into micelles of surfactants, and the partial interaction of TIPB with TPOS causes the decrease in the hydrolysis rate of TPOS, leading to a slight increase in the particle diameter. When $x$ becomes higher ($2 < x \leq 8$), the pore size is not enlarged because there is little space to incorporate TIPB into micelles. The phase separation of TIPB from water and the increase in the interaction of TIPB with TPOS lead to an obvious increase in the particle diameter.

*3.1.3.ii 8 < x ≤ 20.* In the cases of $8 \leq x \leq 20$, the pore size of P_TIPB*x*-as decreased and the particle diameter clearly increased. Nitrogen adsorption–desorption isotherms (Fig. S8†) show that the mesostructure changed. This variation should be due to the relatively large amount of oil (including TIPB) and also due to the formation of complicated emulsion consisting of water, oil, and surfactants.[92] In the present case, the presence of an excess amount of TIPB varied the structures of micelles, siliceous species, and their composites, probably leading to the variation of the mesostructure. Thus, the pore size was not enlarged and decreased in the range of $8 < x \leq 20$.

In addition, as $x$ increased, the volume of oil increased and the amount of TPOS incorporated into the oil phase also increased. As shown in Scheme 1, the particle was grown successively to 380 nm.

*3.1.3.iii Comparison of the present case with the case of the addition of propanol.* As reported previously,[80,82] the decrease in the hydrolysis rates of alkoxysilanes leads to the enlargement of the particle diameter. In the case of alcohols, it is necessary to add 88 mmol of propanol (using TPOS) in order to enlarge the particle diameter from 40 nm to 80 nm and to add 88 mmol of butanol (using TBOS) to enlarge from 80 nm to 330 nm. On the other hand, in the case of TAB (in particular TIPB), 11 mmol of TIPB can enlarge the particle diameter from 40 nm to 380 nm. That is, the effect of TAB on the enlargement of the particle diameter is much stronger than that of alcohols. It should be ascribed to the lower relative electric permittivity (and thus higher hydrophobicity) of TAB than that of butanol (water: 80, TAB: 2–2.3, and butanol: 18). This means that TAB delays the hydrolysis of alkoxysilanes more effectively than alcohols, followed by particle growth more dominant than nucleation.

### 3.2 Preparation of CMSS and CMPS by adding TMB

**3.2.1 Characterization of P_TMB*x*-as and P_TMB*x*-dia.** Similar to the cases of TIPB, the appearance of P_TMB0.8-dia was almost transparent with a slightly blue color, and with a clear Rayleigh scattering, as shown in Fig. S10b† insets. From the DLS measurement of P_TMB0.8-dia (Fig. S11†), aggregates larger than 1000 nm in size were not observed and a single peak was observed near 100 nm, which means that the nanoparticles are dispersed in an aqueous medium. The nanoparticles with *ca.* 100 nm in size were also observed from the SEM images (Fig. S10b and S10f†). In each case of $0 \leq x \leq 8$, the aqueous dispersity of particles was confirmed (data not shown).

The SEM image of P_TMB0.8-dia also shows that the pore size is *ca.* 4 nm and that this value was similar to that of P-dia which were made without the addition of trialkylbenzenes (Fig. S10a and S10d†). The $N_2$ adsorption–desorption isotherms of the cases using TMB show that the values of $P/P_0$ corresponding to capillary condensation are around 0.4 and that these are similar to that of P-dia (Fig. S12†). Besides, in the cases of P_TMB*x*-dia ($0 \leq x \leq 0.8$), the pore sizes were almost constant and independent of the values of $x$ and the distinct enlargement of the pore size according to the increase in the value of $x$ was not observed (Fig. S13†). On the other hand, in the cases of P_TIPB*x*-dia ($0 \leq x \leq 0.8$), the relative pressures ($P/P_0$) corresponding to capillary condensation were high (around 0.7), showing the enlargement of the pore size with the increase in the value of $x$.

The reason for the difference in the enlargement of the pore size among various kinds of trialkylbenzenes was discussed in the previous report by Fukuoka *et al.*[91] It is described that in the case of mesoporous silica made from CTAB micelles and trialkylbenzenes, the position of trialkylbenzenes in micelles is a key factor for pore size enlargement. On the basis of this report, the behavior of the formation of micelles is described as follows. Because the structure of TMB is planar, a number of TMB molecules can get into the space between surfactant molecules in micelles (Scheme 2b), thus micelles should not be enlarged clearly when the additional amount of TMB increases. On the other hand, because the bulkiness of TIPB is larger than that of TMB, lesser amounts of TIPB should exist in the spaces between surfactants in micelles. Thus, it should be easy for TIPB to get into the hydrophobic central space of micelles (Scheme 2c). For this reason, the additional amount of TIPB led to the increased accumulation in the hydrophobic center of micelles and the distinct enlargement of micelles.

When the amount of TMB was increased ($x = 20$), radial mesopores were observed from the TEM image and the size of mesopores was dozens of nanometers, as shown in the SEM image (Fig. 4). The XRD pattern of the dried sample (P_TMB20-dia) showed a very broad peak and a peak due to mesostructures was not confirmed clearly (Fig. S14†). The reason for the formation of particles with large radial mesopores will be discussed in the next section on the basis of several previous reports about particles with similar structures.

**3.2.2 Effect of the kind of trialkylbenzene on the mesostructure and particle morphology.** The differences in the mesostructure and particle morphology can be explained by how TAB interacts with surfactants. On the basis of higher swelling ratios of HDPE for TMB than that for TIPB (Table S1†), TMB should easily diffuse between the alkyl chains of surfactants, while TIPB tends to assemble in the core

 

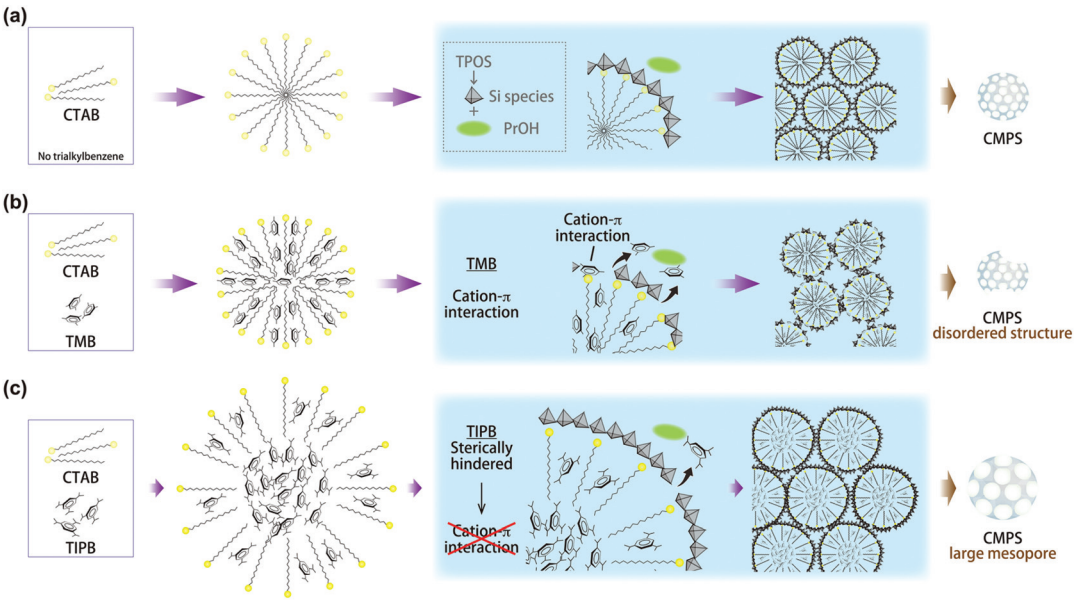


**Scheme 2** Proposed structures of micelles and formation of CMPS; (a) without TAB, (b) with TMB, and (c) with TIPB.

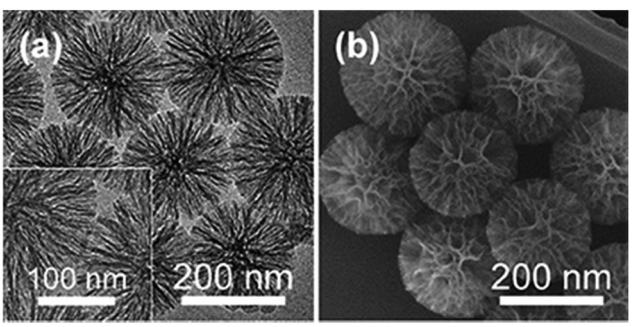


**Fig. 4** (a) TEM and (b) SEM images of P_TMB20-dia.

of micelles (Scheme S2†). Such a difference in the swelling behaviors will be used for discussion in the following paragraphs.

In order to obtain MSN with radial pores, typically shown in Fig. 4, the following two points are important, that is (1) suppression of the adsorption of soluble silica species on the micelles of surfactants and (2) the release of TAB encapsulated in the micelles to vary the micelle-directed mesostructure. On the basis of this consideration, it has been reported that TMB can have cation–π interactions with the head groups of surfactants as well as hydrophobic interactions with the alkyl chains of surfactants.[89,93] It was also reported that the cation–π interaction becomes stronger in an aqueous system.[94] Thus, in the present system, the phenomenon (1) must have occurred because the adsorption of soluble silica species on the head groups of surfactants is hindered due to the cation–π interaction between TMB and surfactants. In the case of $x$ = 0.8, particles with a disordered morphology were obtained (Fig. S10†). This should be ascribed to the adsorption of TMB on micelles in competition with soluble silica species, therefore, the contact points of silica species with surfactants are heterogeneously limited. Moreover, in terms of case (2), TMB should exist in the state as shown in Scheme 2b and TMB near the outer surface of micelles can come into contact with solvents. In addition, TMB should be more soluble gradually in the aqueous phase because the hydrophobicity of solvents increases due to the presence of propanol generated from the hydrolysis of TPOS. For these reasons, TMB can leak and diffuse from the inner space of micelles to the outer (but still inside) space to make the shape of micelles larger along the axis of rod-like micelles.

On the other hand, as shown in Scheme 2c, TIPB should exist in the inner space of micelles and it is less likely for TIPB to make contact with solvents in the outer space of micelles. Thus, compared to the case of TMB, TIPB should be less affected by the hydrophobization of solvents due to the presence of propanol (derived from TPOS) and be less likely to leak and diffuse to the outside of micelles. It should lead to the suppression of the formation of large radial pores as found for the case of TMB. In addition, the steric hindrance of TIPB is larger than that of TMB, and thus the cation–π interaction between the head groups of surfactants and TIPB should be less likely. On the basis of this consideration, it can be explained that spherical particles were obtained in the case of $x$ = 0.8 because the adsorption of soluble silica species on micelles is thought to occur in a relatively homogeneous way (Scheme 2b).

Moreover, it should be noted that the volume of TIPB is about twice larger than that of TMB at the same molar concentration. This means TIPB can have a stronger effect on expanding the size of micelles than TMB, regardless of how TAB interacts with surfactants. However, in the present case, the

expansion by TIPB (*ca.* 4 nm to 8 nm, in the range of $0 \leq x \leq 0.8$) occurred clearly, while the expansion by TMB was not observed (almost the same *ca.* 4 nm, in the range of $0 \leq x \leq 0.8$). Thus, it is shown that relative locations of TAB and micelles have a greater influence on the expansion of pore size than the difference in volumes of TAB.

Consequently, the effects of the kind of TAB on the preparation of CMSS and CMPS can be summarized in the following three points: (i) regardless of the kind of TAB, colloidal mesoporous silica nanoparticles dispersed in aqueous solution can be prepared, (ii) in the case of TIPB, the pore size of CMPS can be controlled easily with the amount of TIPB, and (iii) by varying the kind of TAB, the mesostructures of CMSS and CMPS can be changed. These phenomena are explained by the steric hindrance and hydrophobicity of TAB, that is, relative locations of TAB and micelles. Such relationship should affect the mesostructure as well as the particle morphology of CMSS.

### 3.3 Pore size enlargement of colloidal mesoporous silica nanoparticles with small particle diameters

By using TIPB, the enlargement of the pore size of small CMPS (20 nm) was investigated. In terms of particle diameter, it was observed by using SEM image (Fig. 5) that the particle diameters of both M-dia and M_TIPB-dia were about 20 nm regardless of the presence of TIPB. Aggregates were not observed apparently. However, as shown in particle size distributions measured by DLS (Fig. 5), the hydrodynamic diameter was about 40 nm and this means that the secondary particles were partly formed by the aggregation of the primary particles.

It was confirmed by the $N_2$ adsorption–desorption isotherms (Fig. S15†) that the pore size of M-dia, which was prepared without the addition of TIPB, was about 4 nm. On the other hand, in the case of M_TIPB-dia, the pore size was about 5 nm. The degree of the enlargement for the cases of M-dia and M_TIPB-dia (from *ca.* 4 nm (M-dia) to *ca.* 5–8 nm (M_TIPB-dia)) is less than that of P-dia and P_TIPB0.8-dia (from *ca.* 4 nm to *ca.* 7 nm). The state and composition of the solution before the addition of Si sources are similar to those of P_TIPB0.8-as, and the micelle size of M_TIPB-as should be about 7 nm. In view of the fact that the particle diameter was about 20 nm, the size of micelles and pore size (*ca.* 5–8 nm) are too large to form particles. Thus, all surfaces of micelles did not contribute to the formation of the framework of particles but a part of surfaces contributed to form the framework, leading to the formation of a silica nanostructure with concave surfaces.

The characteristics of silica nanostructures with concave surfaces are explained as follows. In the step of the preparation of mesostructured silica nanoparticles, the structure which consists of several micelles of surfactants, corresponds to the structure in the initial step of nucleation. Taking into account the mechanism proposed by Hollamby,[95] several species of silicate–surfactant composite micelles are formed in the initial step of nucleation of mesostructured silica nanoparticles. As shown in Scheme 3, the proposed model is applied to the present case judging from the size of micelles and the particle diameter of CMSS. This means that the silica nanostructure with concave surfaces in this case is comparable to particles in the initial step of nucleation. The present mesostructured and mesoporous nanoparticles with concave surfaces had much smaller particle diameter and the curvature of concaves was smaller than those reported previously on MSN.[81,95] These particles should contribute to the development of siliceous materials which have both convex and concave surfaces for various applications of catalysis and drug delivery.

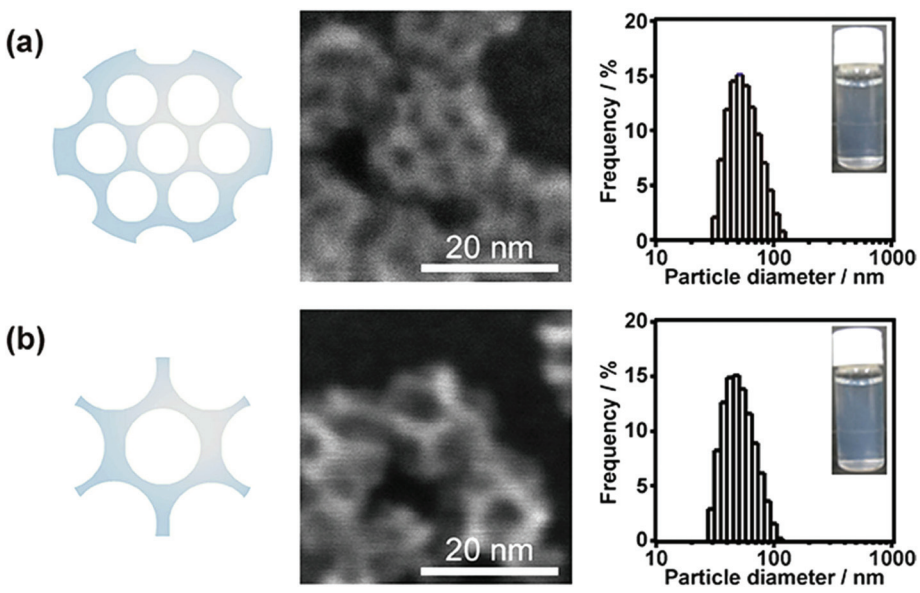


Fig. 5 Schematic images, SEM images, appearances, and the particle size distributions (DLS, hydrodynamic diameter) of (a) M-dia and (b) M_TIPB-dia.

 

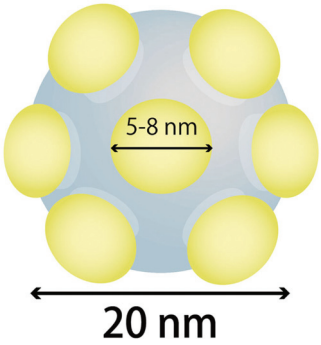


**Scheme 3** Proposed model of M_TIPB-as, which was prepared by using TIPB as TAB and using TMOS as a Si source. Gray: siloxane frameworks, yellow: micelles embedded in the siloxane frameworks.

## 4. Conclusion

Aqueous colloidal mesostructured silica nanoparticles (CMSS) were prepared by varying the kind and amount of trialkylbenzenes (TAB) and by varying Si sources. When 1,3,5-triisopropylbenzene (TIPB) was used as TAB and tetrapropoxysilane (TPOS) was used as a Si source, both the pore size (from 4 nm to 8 nm) and particle diameter (from 50 nm to 380 nm) were enlarged with the amount of TIPB. In the case of TPOS and an excess amount of 1,3,5-trimethylbenzene (TMB), the pore size of CMSS was also enlarged above 10 nm, accompanied by the variation of the mesostructure and deformation of the spherical morphology. When tetramethoxysilane and TIPB were used, CMSS with a small particle diameter (20 nm), concave surfaces, and a large pore size (5–8 nm) were obtained, which should be equivalent to particles formed at the initial nucleation. TIPB can enlarge the pore size and particle diameter than TMB, and the enlargement by TIPB was accomplished without the variation of the mesostructure and particle morphology. This should be ascribed to the larger size and higher hydrophobicity of TIPB than those of TMB. Besides, removal of surfactants and TAB by a dialysis process was successful for the preparation of aqueous highly dispersed colloidal mesoporous silica nanoparticles with enlarged pores. The present findings will lead to the development of siliceous materials which can accommodate more guest molecules with a larger size, and they can expand possible applications for drug delivery and bioimaging as well as catalysis and concomitantly can reduce their nanorisks.

## Acknowledgements

The authors thank Mr M. Fuziwara (Waseda University) for his kind assistance in TEM measurement. This work was supported in part by Grant-in-Aid for Scientific Research, MEXT (15K13809).

## References

1 V. Valtchev and L. Tosheva, *Chem. Rev.*, 2013, **113**, 6734–6760.
2 S.-H. Wu, C.-Y. Mou and H.-P. Lin, *Chem. Soc. Rev.*, 2013, **42**, 3862–3875.
3 C. E. Fowler, D. Khushalani, B. Lebeau and S. Mann, *Adv. Mater.*, 2001, **13**, 649–652.
4 S. Sadasivan, C. E. Fowler, D. Khushalani and S. Mann, *Angew. Chem., Int. Ed.*, 2002, **41**, 2151–2153.
5 H.-P. Lin and C.-P. Tsai, *Chem. Lett.*, 2003, 1092–1093.
6 J. Fan, J. Lei, L. Wang, C. Yu, B. Tu and D. Zhao, *Chem. Commun.*, 2003, 2140–2141.
7 K. Suzuki, K. Ikari and H. Imai, *J. Am. Chem. Soc.*, 2004, **126**, 462–463.
8 K. Möller, J. Kobler and T. Bein, *Adv. Funct. Mater.*, 2007, **17**, 605–612.
9 J. Kobler and T. Bein, *ACS Nano*, 2008, **2**, 2324–2330.
10 A. Berggren and A. E. C. Palmqvist, *J. Phys. Chem. C*, 2008, **112**, 732–737.
11 F. Lu, S.-H. Wu, Y. Hung and C.-Y. Mou, *Small*, 2009, **5**, 1408–1413.
12 Y.-S. Lin, N. Abadeer and C. L. Haynes, *Chem. Commun.*, 2011, **47**, 532–534.
13 Y.-S. Lin, N. Abadeer, K. R. Hurley and C. L. Haynes, *J. Am. Chem. Soc.*, 2011, **133**, 20444–20457.
14 K. Ma, H. Sai and U. Wiesner, *J. Am. Chem. Soc.*, 2012, **134**, 13180–13183.
15 K. Ma, U.-W. Zwanziger, J. Zwanziger and U. Wiesner, *Chem. Mater.*, 2013, **25**, 677–691.
16 D. Douroumis, I. Onyesom, M. Maniruzzaman and J. Mitchell, *Crit. Rev. Biotechnol.*, 2013, **33**, 229–245.
17 M. Bouchoucha, R. C. Gaudreault, M.-A. Fortin and F. Kleitz, *Adv. Funct. Mater.*, 2014, **24**, 5911–5923.
18 S. M. Egger, K. R. Hurley, A. Datt, G. Swindlehurst and C. L. Haynes, *Chem. Mater.*, 2015, **27**, 3193–3196.
19 K. K. Unger, D. Kumar, M. Grün, G. Büchel, S. Lüdtke, T. Adam, K. Schumacher and S. J. Renker, *J. Chromatogr., A*, 2000, **892**, 47–55.
20 S. H. Joo, J. Y. Park, C. K. Tsung, Y. Yamada, P. D. Yang and G. A. Somorjai, *Nat. Mater.*, 2009, **8**, 126–131.
21 Y.-S. Lin, K. R. Hurley and C. L. Haynes, *J. Phys. Chem. Lett.*, 2012, **3**, 364–374.
22 K. C.-W. Wu and Y. Yamauchi, *J. Mater. Chem.*, 2012, **22**, 1251–1256.
23 X. Li, J. C. Barnes, A. Bosoy, J. F. Stoddart and J. I. Zink, *Chem. Soc. Rev.*, 2012, **41**, 2590–2605.
24 J. L. Vivero-Escoto, R. C. H. Phillips and W. Lin, *Chem. Soc. Rev.*, 2012, **41**, 2673–2685.
25 P. Yang, S. Gai and J. Lin, *Chem. Soc. Rev.*, 2012, **41**, 3679–3698.
26 P. Nadrah, O. Planinšek and M. Gaberšček, *J. Mater. Sci.*, 2014, **49**, 481–495.
27 X. Huang, N. P. Young and H. E. Townley, *Nanomater. Nanotechnol.*, 2014, **4**, 1–15.
28 L. Cheng, C. Wang, L. Feng, K. Yang and Z. Liu, *Chem. Rev.*, 2014, **114**, 10869–10939.
29 Y. Chen, H. Chen and J. Shi, *Expert Opin. Drug Delivery*, 2014, **11**, 917–930.
30 P. Xu, S. Guo, H. Yu and X. Li, *Small*, 2014, **10**, 2404–2412.

31 X. Wang, H. Chen, K. Zhang, M. Ma, F. Li, D. Zeng, S. Zheng, Y. Chen, L. Jiang, H. Xu and J. Shi, *Small*, 2014, **10**, 1403–1411.
32 R. Roggers, S. Kanvinde, S. Boonsith and D. Oupický, *AAPS PharmSciTech.*, 2014, **15**, 1163–1171.
33 I. Sierra, D. P. Quintanilla, S. Morante and J. Gañán, *J. Chromatogr., A*, 2014, **1363**, 27–40.
34 S. A. Jadhav, *Inorg. Chem. Front.*, 2014, **1**, 735–739.
35 C. Argyo, V. Weiss, C. Brauchle and T. Bein, *Chem. Mater.*, 2014, **26**, 435–451.
36 Y. Zhang, B. Y. W. Hsu, C. Ren, X. Li and J. Wang, *Chem. Soc. Rev.*, 2015, **44**, 315–335.
37 N. Song and Y.-W. Yang, *Chem. Soc. Rev.*, 2015, **44**, 3474–3504.
38 M. Wang, Z. Sun, Q. Yue, J. Yang, X. Wang, Y. Deng, C. Yu and D. Zhao, *J. Am. Chem. Soc.*, 2014, **136**, 1884–1892.
39 Q. Qu, G. Zhou, Y. Ding, S. Feng and Z. Gu, *J. Non-Cryst. Solids*, 2014, **405**, 104–115.
40 X. Du and S. Z. Qiao, *Small*, 2015, **11**, 392–413.
41 X. Ma, K. Hahn and S. Sanchez, *J. Am. Chem. Soc.*, 2015, **137**, 4976–4979.
42 H. Ishii, T. Ikuno, A. Shimojima and T. Okubo, *J. Colloid Interface Sci.*, 2015, **448**, 57–64.
43 S. Rashi, S. K. Prajapati and D. Singh, *World J. Pharm. Pharm. Sci.*, 2015, **4**, 332–347.
44 G. Chen, Z. Teng, X. Su, Y. Liu and G. Lu, *J. Biomed. Nanotechnol.*, 2015, **11**, 1–8.
45 Y. Chen, H. Chen and J. Shi, *Adv. Healthcare Mater.*, 2015, **4**, 158–165.
46 Z. Ma, J. Bai, Y. Wang and X. Jiang, *ACS Appl. Mater. Interfaces*, 2014, **6**, 2431–2438.
47 S. B. Hartono, M. Yu, W. Gu, J. Yang, E. Strounina, X. Wang, S. Qiao and C. Yu, *Nanotoxicology*, 2014, **25**, 1–12.
48 D. Niu, Z. Liu, Y. Li, X. Luo, J. Zhang, J. Gong and J. Shi, *Adv. Mater.*, 2014, **26**, 4947–4953.
49 Z. Gao and I. Zharov, *Chem. Mater.*, 2014, **26**, 2030–2037.
50 J. Peng, J. Liu, J. Liu, Y. Yang, C. Li and Q. Yang, *J. Mater. Chem. A*, 2014, **2**, 8118–8125.
51 L. Miller, G. Winter, B. Baur, B. Witulla, C. Solbach, S. Reske and M. Lindén, *Nanoscale*, 2014, **6**, 4928–4935.
52 X. Ye, J. Wang, Y. Xu, L. Niu, Z. Fan, P. Gong, L. Ma, H. Wang, Z. Yang and S. Yang, *J. Appl. Polym. Sci.*, 2014, **131**, 41173.
53 M. Wu, Q. Meng, Y. Chen, Y. Du, L. Zhang, Y. Li, L. Zhang and J. Shi, *Adv. Mater.*, 2015, **27**, 215–222.
54 N. Ž. Knežević and J.-O. Durand, *Nanoscale*, 2015, **7**, 2199–2209.
55 H. Vallhov, S. Gabrielsson, M. Strømme, A. Scheynius and A. E. G. Bennett, *Nano Lett.*, 2007, **7**, 3576–3582.
56 D. Napierska, C. J. Thomassen, V. Rabolli, D. Lison, L. Gonzalez, M. K. Volders, J. A. Martens and P. H. Hoet, *Small*, 2009, **5**, 846–853.
57 F. Lu, S.-H. Wu, Y. Hung and C.-Y. Mou, *Small*, 2009, **5**, 1408–1413.
58 Q. He, Z. Zhang, Y. Gao, J. Shi and Y. Li, *Small*, 2009, **5**, 2722–2729.
59 D. Napierska, L. C. J. Thomassen, D. Lison, J. Martens and P. H. Hoet, *Part. Fibre Toxicol.*, 2010, **7**, 39–70.
60 V. Rabolli, L. C. J. Thomassen, C. Princen, D. Napierska, L. Gonzalez, M. K. Volders, P. H. Hoet, F. Huaux, C. E. A. Kirschhock, J. A. Martens and D. Lison, *Nanotoxicology*, 2010, **4**, 307–318.
61 Y.-S. Lin and C. L. Haynes, *J. Am. Chem. Soc.*, 2010, **132**, 4834–4842.
62 F. Zhao, Y. Zhao, Y. Liu, X. Chang, C. Chen and Y. Zhao, *Small*, 2011, **7**, 1322–1337.
63 D. Shen, J. Yang, X. Li, L. Zhou, R. Zhang, W. Li, L. Chen, R. Wang, F. Zhang and D. Zhao, *Nano Lett.*, 2014, **14**, 923–932.
64 M. Varache, I. Bezverkhyy, L. Saviot, F. Bouyer, F. Baras and F. Bouyer, *J. Non-Cryst. Solids*, 2015, **408**, 87–97.
65 A. B. D. Nandiyanto, S.-G. Kim, F. Iskandar and K. Okuyama, *Microporous Mesoporous Mater.*, 2009, **120**, 447–453.
66 Y. Hoshikawa, H. Yabe, A. Nomura, T. Yamaki, A. Shimojima and T. Okubo, *Chem. Mater.*, 2010, **22**, 12–14.
67 M.-H. Kim, H.-K. Na, Y.-K. Kim, S.-R. Ryoo, H. S. Cho, K. E. Lee, H. Jeon, R. Ryoo and D.-H. Min, *ACS Nano*, 2011, **5**, 3568–3576.
68 V. Polshettiwar, D. Cha, X. Zhang and J. M. Basset, *Angew. Chem., Int. Ed.*, 2010, **49**, 9652–9656.
69 S.-M. Lai, H.-Y. Lai and M.-Y. Chou, *Microporous Mesoporous Mater.*, 2014, **196**, 31–40.
70 Q. Cai, Z.-S. Luo, W.-Q. Pang, Y.-W. Fan, X.-H. Chen and F.-Z. Cui, *Chem. Mater.*, 2001, **13**, 258–263.
71 T. Yokoi, T. Karouji, S. Ohta, J. N. Kondo and T. Tatsumi, *Chem. Mater.*, 2010, **22**, 3900–3908.
72 J. Wang, A. S. Narutaki, A. Shimojima and T. Okubo, *J. Colloid Interface Sci.*, 2012, **385**, 41–47.
73 K.-C. Kao and C.-Y. Mou, *Microporous Mesoporous Mater.*, 2013, **169**, 7–15.
74 G. Sponchia, R. Marin, I. Freris, M. Marchiori, E. Moretti, L. Storaro, P. Canton, A. Lausi, A. Benedetti and P. Riello, *J. Nanopart. Res.*, 2014, **16**, 1–14.
75 A. B. Fuertes, P. V. Vigón and M. Sevilla, *J. Colloid Interface Sci.*, 2010, **349**, 173–180.
76 J. S. Beck, J. C. Vartuli, W. J. Roth, M. E. Leonowicz, C. T. Kresge, K. D. Schmitt, C. T. W. Chu, D. H. Olson, E. W. Sheppard, S. B. McCullen, J. B. Higgins and J. L. Schlenker, *J. Am. Chem. Soc.*, 1992, **114**, 10834–10843.
77 N. Ulagappan and C. N. R. Rao, *Chem. Commun.*, 1996, 2759–2760.
78 M. Luechinger, G. D. Pirngruber, B. Lindlar, P. Laggner and R. Prins, *Microporous Mesoporous Mater.*, 2005, **79**, 41–52.
79 Y. Zhang, H. Zhang, E. Che, L. Zhang, J. Han, Y. Yang, S. Wang, M. Zhang and C. Gao, *Colloids Surf., B*, 2015, **128**, 77–85.
80 H. Yamada, C. Urata, H. Ujiie, Y. Yamauchi and K. Kuroda, *Nanoscale*, 2013, **5**, 6145–6153.
81 C. Urata, Y. Aoyama, A. Tonegawa, Y. Yamauchi and K. Kuroda, *Chem. Commun.*, 2009, 5094–5096.

82 H. Yamada, C. Urata, Y. Aoyama, S. Osada, Y. Yamauchi and K. Kuroda, *Chem. Mater.*, 2012, **24**, 1462–1471.
83 H. Yamada, C. Urata, S. Higashitamori, Y. Aoyama, Y. Yamauchi and K. Kuroda, *ACS Appl. Mater. Interfaces*, 2014, **6**, 3491–3500.
84 C. Urata, H. Yamada, R. Wakabayashi, Y. Aoyama, S. Hirosawa, S. Arai, S. Takeoka, Y. Yamauchi and K. Kuroda, *J. Am. Chem. Soc.*, 2011, **133**, 8102–8105.
85 E. Yamamoto, M. Kitahara, T. Tsumura and K. Kuroda, *Chem. Mater.*, 2014, **26**, 2927–2933.
86 H. Ujiie, A. Shimojima and K. Kuroda, *Chem. Commun.*, 2015, **51**, 3211–3214.
87 H. Yamada, C. Urata, E. Yamamoto, S. Higashitamori, Y. Yamauchi and K. Kuroda, *ChemNanoMat*, 2015, **1**, 194–202.
88 M. Tiemann, V. Goletto, R. Blum, F. Babonneau, H. Amenitsch and M. Lindén, *Langmuir*, 2002, **18**, 10053–10057.
89 J. L. Blin and B. L. Su, *Langmuir*, 2002, **18**, 5303–5308.
90 H. Kunieda, K. Ozawa and K. L. Huang, *J. Phys. Chem. B*, 1998, **102**, 831–838.
91 A. Fukuoka, I. Kikkawa, Y. Sasaki, A. Shimojima and T. Okubo, *Langmuir*, 2009, **25**, 10992–10997.
92 D.-S. Moon and J.-K. Lee, *Langmuir*, 2012, **28**, 12341–12347.
93 M. F. Ottaviani, A. Moscatelli, D. D. Giscard, F. D. Renzo, P. J. Kooyman, B. Alonso and A. Galarneau, *J. Phys. Chem. B*, 2004, **108**, 12123–12129.
94 J. P. Gallivan and D. A. Dougherty, *J. Am. Chem. Soc.*, 2000, **122**, 870–874.
95 M. J. Hollamby, D. Borisova, P. Brown, J. Eastoe, I. Grillo and D. Shchukin, *Langmuir*, 2012, **28**, 4425–4433.